JOURNAL OF GUIDANCE, CONTROL, AND DYNAMICS
Vol. 21, No. 2, March–April 1998

Three-Dimensional Hinged-Rod Model for Elastic Aerobraking Tethers

Brian L. Biswell* and Jordi Puig-Suari†
Arizona State University, Tempe, Arizona 85287-6106
and
James M. Longuski‡ and Steven G. Tragesser§
Purdue University, West Lafayette, Indiana 47907-1282

Earlier analysis with a rigid-rod model demonstrated that aerobraking tethers are feasible. In fact, the aerobraking tether may be superior to chemical retropropulsion when applied to exploration of the atmosphere-bearing planets of the solar system. Recent optimization studies provide even further advances in minimizing the tether mass with respect to propellant mass. Inasmuch as most of the work performed so far has modeled the tether as a rigid rod, it is clear that bending effects warrant investigation. An advanced model, consisting of a collection of hinged rigid bodies with springs and dampers at the hinges, is introduced. By using a matrix formulation the equations can be made very compact for any number of tether segments. The orbiter and probe vehicles at the ends of the tether are also modeled as rigid bodies with the added feature of a movable attachment point. The forces include distributed gravitational and aerodynamic forces over the entire tether. A numerical example is presented that uses a prior mass optimization solution (based on the planar, rigid-rod model) for aerobraking at Mars. The example involves capture into an inclined orbit, which creates flexing in both out-of-plane and in-plane motions. The results indicate that the flexible behavior of a carefully designed tether is benign and does not exhibit large perturbations from the rigid-rod behavior. Because of its generality, the new model may prove useful to other investigators working with tethers in space.

I. Introduction

AN aerobraking tether consists of an orbiter and an atmospheric probe, connected by a long thin tether (Fig. 1). The purpose of this system is to achieve aerobraking at an atmosphere-bearing planet in such a way as to eliminate the need for a retropropulsion maneuver. An additional goal is to place the orbiter in a target orbit, sufficiently high above the sensible atmosphere, while the probe performs the braking maneuver. The orbiter is slowed from hyperbolic speed down to capture speed through the tension in the tether, which may be tens or even hundreds of kilometers in length. After aerocapture has been achieved, the tether may be severed to allow the probe to descend farther into the atmosphere (in some cases perhaps to land on the surface) while the orbiter ascends to a higher orbit. Alternatively, the system may be kept together, permitting further aerobraking passes on subsequent orbits.

The first mention of the concept of an aerobraking tether in the literature appears to be by Carroll,[1] although the idea was being discussed at the Jet Propulsion Laboratory at least as early as 1984 by Sirlin et al.[2] Another early reference to the aerobraking tether concept is made by Purvis and Penzo.[3]

The first demonstration of the physical feasibility of using aerobraking tethers is presented by Puig-Suari and Longuski[4] and Longuski and Puig-Suari.[5] They model the tether as a rigid rod subject to distributed aerodynamic and gravitational forces and show that the orbiter altitude can be maintained above the sensible atmosphere during the aerobraking maneuver. Puig-Suari and Longuski use the characteristics of a tethered vehicle described by Lorenzini et al.,[6] which was originally intended for circular orbit about Mars.

Puig-Suari and Longuski[7] analyze the problem of targeting the aerobraking tether to achieve aerocapture for specific closest approach flyby attitudes ranging from an orientation that is locally vertical (called the vertical dumbbell maneuver) to an orientation that is locally horizontal (the drag chute maneuver). Puig-Suari et al.[8] then use the vertical dumbbell maneuver along with design rules of thumb to find unique tether designs for aerobraking at the major atmosphere-bearing bodies of the solar system (Venus, Earth, Mars, Jupiter, Saturn, Titan, Uranus, and Neptune). In the process they demonstrate that (neglecting stochastic effects) the nominal tether mass is significantly lower than the propellant mass required to achieve aerocapture. Longuski et al.[9] demonstrate even greater mass reduction (for the nominal case) by solving the optimum tether mass problem. The resulting aerobraking maneuver is midway between the vertical dumbbell and drag chute maneuvers studied earlier.

All of the analyses for aerobraking tethers mentioned so far are restricted to the rigid-rod assumption. The first attempt to model the flexible behavior of the system is presented by Puig-Suari and Longuski,[10] where they assume that the tether can be modeled as a collection of hinged rigid rods restricted to motion in the orbital plane. However, Puig-Suari[11] demonstrates that the rigid model is still a useful tool in the initial optimization of the aerobraking maneuver and that the optimal flexible tether is near that of the rigid optimum.

In this paper, we present the most versatile and sophisticated model, so far developed, for the aerobraking tether. In the process of developing this model we have kept in mind two major goals, each of which have a number of subsidiary goals.

The first major goal is to obtain the best possible model for the aerocapture problem. To achieve this we wished to model out-of-plane and in-plane flexing of the tether, in addition to the attitude dynamics of the endpoints. The second major goal is to extend the aerocapture model to include, as much as possible, some of the phenomena being studied by other researchers in tethers in space.[12] This extension is by no means intended to be complete but because of the advantages of the hinged rigid-body model (over, e.g., the bead models) and the very compact form realized by the matrix formulation, we feel that this effort will be beneficial in studying tethered spacecraft attitude control problems,[13–18] tether equilibrium and stability problems,[19–21] tethers in an atmosphere,[22–25] tether orbit decay,[26]

Received May 6, 1997; revision received Oct. 3, 1997; accepted for publication Oct. 4, 1997.

*Ph.D. Candidate, Department of Mechanical and Aerospace Engineering. Student Member AIAA.
†Assistant Professor, Department of Mechanical and Aerospace Engineering. E-mail: jordi@asu.edu. Member AIAA.
‡Associate Professor, School of Aeronautics and Astronautics. Associate Fellow AIAA.
§Ph.D. Candidate, School of Aeronautics and Astronautics. Student Member AIAA.

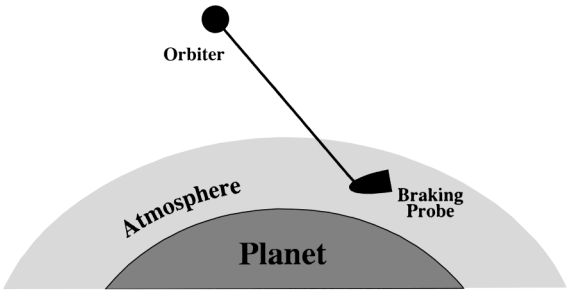

Fig. 1 Aerobraking maneuver.

tether vibrations,[27–29] tether flight experiments,[30–32] and other tether control and dynamics problems.[33] Problems involving nonspherical planets[34] or tether deployment and retrieval[35,36] are not addressed here, but the model provided could serve as a basis for these more difficult problems.

We mention, in passing, that very complex simulation tools do exist for tether dynamics. Perhaps most notable of these is Generalized Tether Object Simulation Systems (GTOSS) by Lang.[37] For general complex motion, such programs are probably the best representation of the actual dynamics. In the case of orbiting tethers in an atmosphere, however, we believe that the formulation of our paper more accurately represents the aerodynamic and gravitational forces acting on the system. The bead model approach used in Lang's program concentrates the gravitational and aerodynamic forces on the discrete bead elements with large gaps between the beads where no forces act. To better model the distributed gravity and aerodynamic effects using the bead model, the only recourse seems to be to add more beads, which unfortunately drives the number of generalized coordinates (the order of the model) to high values, with the unavoidable consequence of slowing down the simulation. Our new model is based on rigid-body elements that incorporate distributed aerodynamic and gravitational forces over the element. With the rigid body as an element, one can often achieve very good results with a much lower-order model (perhaps even a single body) as demonstrated in the orbit decay analysis of Warnock and Cochran.[26] In cases in which aerodynamic effects are inconsequential, the rigid-body model may still have advantages over the bead model, particularly when the tether mass cannot be neglected. It remains to be seen, in actual simulation comparison, to what degree the effects of distributed gravitational and aerodynamic forces are best modeled by rigid bodies as opposed to beads.

There is one final advantage that our model possesses over the very complex models: the compactness of the equations. This paper contains the complete model (for a single tether). The equations are in a form eminently suited for structured programming. The compact and explicit nature of these equations makes the modeling assumptions clear and provides a straightforward basis for extensions of the model. (The equations of the GTOSS model are handwritten in Volume 11 of the user's guide[37] and occupy 246 pages.) It should be stressed, however, that GTOSS is capable of simulating the behavior of up to nine rigid-body objects interconnected in any conceivable fashion at eight attachment points per body with a grand total of 25 tethers. The program is quite lengthy: 40,000 lines of source code. The tether model presented in this paper is quite modest by comparison and only involves one tether and two rigid-body endpoints. However, we believe that the model will help bridge the gap between highly simplified tether models, e.g., rigid rod in circular orbit and the highly complex simulations of GTOSS.

II. Modeling Assumptions

The tether system is represented by a collection of hinged rigid bodies connected by springs and dampers. The orbiter and probe are assumed to be rigid bodies with three rotational degrees of freedom each. The tether segments are also assumed to be rigid bodies (for the sake of structural similarity in the equations of motion) but the mass of each segment is distributed into two point masses placed to duplicate the inertia properties of the rigid rod. The distribution of the tether mass in this manner duplicates the gravity forces and moments of the rigid rod to within 1% error. The orientation of each rigid body in the system is given by the Euler angle sequence 3–2–1 with respect to the probe frame $\hat{\boldsymbol{p}}$. Whereas all three Euler angles are important in the case of the orbiter and the probe, we see that, in the case of a tether segment, the third Euler angle rotation is meaningless, because it represents rotation along the symmetry axis of a long thin rod.

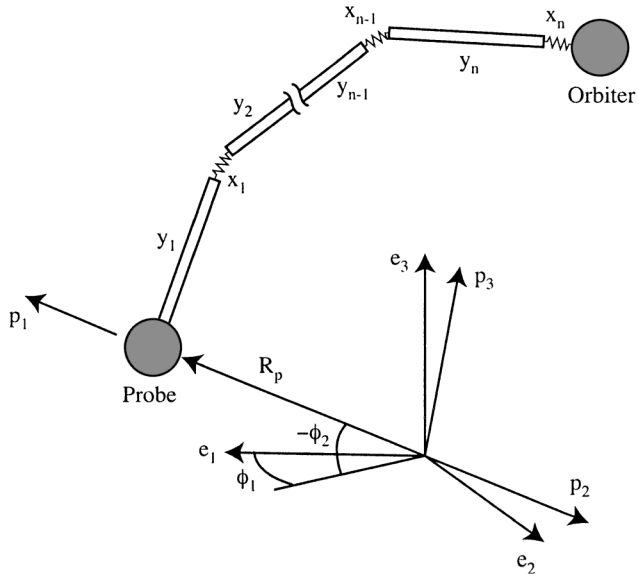

Fig. 2 Three-dimensional flexible–elastic tether model.

Figure 2 shows an arbitrary configuration of the tether model. The inertial coordinate system $\hat{\boldsymbol{e}}$ is located at the center of mass of the planet. The first reference body of the tether is the probe, whose position is given by $R_p\hat{\boldsymbol{p}}_1$, where R_p is the distance from the origin to the center of mass of the probe and $\hat{\boldsymbol{p}}_1$ is a unit vector that points at the probe from the center of the planet.

The forces on the tethered system are assumed to be gravity and drag. The tether segments are not assumed to be massless, and it is clear that in the case of very long tether segments that the gravitational force at each point of the tether can vary because of distance. In this model we will adopt Newton's inverse square law ($F_G = GMm/R^2$) which, for a pure rigid rod, necessitates integrating the force of gravity over the entire segment. Puig-Suari et al.[38] demonstrated that integrating the gravity force over the entire element, although yielding the most accurate results, introduces a numerical singularity that can be solved at the cost of increased computation time. To remove this problem, we concentrate the mass of each tether element into two point masses located so that the element has the same moment of inertia as a uniform rod and so that it reasonably models the gravitational forces and moment on the rod without extended computation time. We note that the atmospheric drag at each point on the tether will vary according to altitude in the atmosphere and the wind speed. Thus, the atmospheric drag must be integrated along the length of each tether segment. Here we assume a velocity squared drag law ($F_D = \frac{1}{2}C_D S v^2$) with a uniform exponential density function ($\rho = \rho_o e^{h/H}$), although more advanced atmospheric models could be applied. In addition, we assume that the atmosphere rotates with the planet.

The tether segments have fixed lengths but each can be different (y_i) and each has a linear spring–damper at the top (with different spring and damping constants k_i and c_i), which remains aligned with the segment. Generally, the spring constants are chosen to satisfy $k_i = EA_i/l_i$, where E is Young's modulus of the tether material and A_i and l_i are the element cross-sectional area and length, respectively. The damping constant is chosen to provide the equivalent structural damping. When the springs stretch (x_i), there is a gap between the segments so that no atmospheric drag is modeled in that region. However it is expected that these gaps will be insignificant in comparison to the area occupied by the segments (and we note that in the case of bead models the problem is exaggerated to the greatest degree). The springs are allowed to have unstretched lengths (u_i). Note that torsional springs have been omitted from the model because the bending resistance of the tether is negligible.

It is interesting to note that this model can be made to emulate the bead model by making the unstretched lengths large and the segment lengths very short. This provides an opportunity to test the model against existing bead models. It is also notable that the springs and dampers are easily removed from the system so that a collection of hinged rigid rods can be simulated. If, in addition, the system is confined to planar motion, the model of Puig-Suari and Longuski[10] can be used for comparison.

The final modeling assumption is that the tether attachment points on the orbiter and the probe are movable so that tethered satellite attitude control systems can be studied with the resulting model, as mentioned earlier.[39]

III. Equations of Motion

The equations of motion for the system are derived using Lagrange's equations, which for a generalized coordinate q_i can be written as

$$\frac{\mathrm{d}}{\mathrm{d}t}\left(\frac{\partial T}{\partial \dot{q}_i}\right) - \frac{\partial T}{\partial q_i} + \frac{\partial V}{\partial q_i} = Q_i \tag{1}$$

where T and V represent the kinetic and potential energy of the system, respectively, and the Q_i are the generalized forces arising from forces not derivable from a potential function.

A. Kinetic Energy

For each one of the bodies in the tethered system, the kinetic energy is

$$T = \tfrac{1}{2}m\{\boldsymbol{v}\}^T\{\boldsymbol{v}\} + \tfrac{1}{2}\{\boldsymbol{\omega}\}^T[\boldsymbol{I}]\{\boldsymbol{\omega}\} \tag{2}$$

where $\{\boldsymbol{v}\}$ is the velocity of the c.m., $\{\boldsymbol{\omega}\}$ is the inertial angular velocity, and $[\boldsymbol{I}]$ is the inertia matrix.

The c.m. positions of the probe and orbiter in the $\hat{\boldsymbol{p}}$ frame are

$$\begin{aligned}\{\boldsymbol{R}_p\} &= R_p\hat{\boldsymbol{p}}_1 \\ \{\boldsymbol{R}_o\} &= \{\boldsymbol{R}_p\} + [\boldsymbol{T}]_p\{\boldsymbol{r}_p\} + \sum_{k=1}^{N}[\boldsymbol{T}]_k\{\boldsymbol{l}_k\} + [\boldsymbol{T}]_o\{\boldsymbol{r}_o\}\end{aligned} \tag{3}$$

and the positions of the two mass elements and c.m. of the ith rod (in the $\hat{\boldsymbol{p}}$ frame) are

$$\begin{aligned}\{\boldsymbol{R}_{ic}\} &= \{\boldsymbol{R}_p\} + [\boldsymbol{T}]_p\{\boldsymbol{r}_p\} + \sum_{k=1}^{i-1}[\boldsymbol{T}]_k\{\boldsymbol{l}_k\} + \frac{1}{2}[\boldsymbol{T}]_i\{\boldsymbol{y}_i\} \\ \{\boldsymbol{R}_{i1}\} &= \{\boldsymbol{R}_p\} + [\boldsymbol{T}]_p\{\boldsymbol{r}_p\} + \sum_{k=1}^{i-1}[\boldsymbol{T}]_k\{\boldsymbol{l}_k\} + \frac{3-\sqrt{3}}{6}[\boldsymbol{T}]_i\{\boldsymbol{y}_i\} \\ \{\boldsymbol{R}_{i2}\} &= \{\boldsymbol{R}_p\} + [\boldsymbol{T}]_p\{\boldsymbol{r}_p\} + \sum_{k=1}^{i-1}[\boldsymbol{T}]_k\{\boldsymbol{l}_k\} + \frac{3+\sqrt{3}}{6}[\boldsymbol{T}]_i\{\boldsymbol{y}_i\}\end{aligned} \tag{4}$$

where

$$\begin{aligned}\{\boldsymbol{r}\} &= \begin{Bmatrix} r_1 \\ r_2 \\ r_3 \end{Bmatrix}, \qquad \{\boldsymbol{l}_k\} = \begin{Bmatrix} y_k + x_k + u_k \\ 0 \\ 0 \end{Bmatrix} \\ \{\dot{\boldsymbol{x}}_k\} &= \begin{Bmatrix} \dot{x}_k \\ 0 \\ 0 \end{Bmatrix}, \qquad \{\boldsymbol{y}_i\} = \begin{Bmatrix} y_i \\ 0 \\ 0 \end{Bmatrix}\end{aligned} \tag{5}$$

The vector $\{\boldsymbol{r}\}$ is the position of the tether attachment point with respect to the c.m. of the rigid body denoted by the subscript o (orbiter) or p (probe). The positions $\{\boldsymbol{r}_p\}$ and $\{\boldsymbol{r}_o\}$ may be constant or determined by a user-specified control law.

$[\boldsymbol{T}]_k$ is the transformation matrix from a frame fixed in the kth body to the probe frame $\hat{\boldsymbol{p}}$:

$$[\boldsymbol{T}]_k = [\boldsymbol{C}_1]_k[\boldsymbol{C}_2]_k[\boldsymbol{C}_3]_k \tag{6}$$

where $[\boldsymbol{C}_i]_k$ is the direction cosine matrix for a rotation about the ith Euler angle of the kth object. Note that, for the tether elements, the twist angle α_3 can be ignored.

Taking derivatives of Eqs. (3) and (4) the corresponding c.m. velocities are

$$\begin{aligned}\{\boldsymbol{v}_p\} &= \{\dot{\boldsymbol{R}}_p\} + [\tilde{\boldsymbol{\omega}}]\{\boldsymbol{R}_p\} \\ \{\boldsymbol{v}_i\} &= \{\dot{\boldsymbol{R}}_p\} + [\dot{\boldsymbol{T}}]_p\{\boldsymbol{r}_p\} + [\boldsymbol{T}]_p\{\dot{\boldsymbol{r}}_p\} \\ &\quad + \sum_{k=1}^{i-1}([\dot{\boldsymbol{T}}]_k\{\boldsymbol{l}_k\} + [\boldsymbol{T}]_k\{\dot{\boldsymbol{x}}_k\}) + \frac{1}{2}[\dot{\boldsymbol{T}}]_i\{\boldsymbol{y}_i\} + [\tilde{\boldsymbol{\omega}}]\{\boldsymbol{R}_{ic}\} \\ \{\boldsymbol{v}_o\} &= \{\dot{\boldsymbol{R}}_p\} + [\dot{\boldsymbol{T}}]_p\{\boldsymbol{r}_p\} + [\boldsymbol{T}]_p\{\dot{\boldsymbol{r}}_p\} \\ &\quad + \sum_{k=1}^{N}([\dot{\boldsymbol{T}}]_k\{\boldsymbol{l}_k\} + [\boldsymbol{T}]_k\{\dot{\boldsymbol{x}}_k\}) + [\dot{\boldsymbol{T}}]_o\{\boldsymbol{r}_o\} + [\boldsymbol{T}]_o\{\dot{\boldsymbol{r}}_o\} + [\tilde{\boldsymbol{\omega}}]\{\boldsymbol{R}_o\}\end{aligned} \tag{7}$$

where $[\tilde{\boldsymbol{\omega}}]$ is the cross-product matrix for the angular velocity of the $\hat{\boldsymbol{p}}$ frame with respect to the inertial frame and

$$\begin{aligned}[\dot{\boldsymbol{T}}]_k &= -\dot{\alpha}_1[\boldsymbol{D}_1]_k[\boldsymbol{C}_2]_k[\boldsymbol{C}_3]_k \\ &\quad - \dot{\alpha}_2[\boldsymbol{C}_1]_k[\boldsymbol{D}_2]_k[\boldsymbol{C}_3]_k - \dot{\alpha}_3[\boldsymbol{C}_1]_k[\boldsymbol{C}_2]_k[\boldsymbol{D}_3]_k\end{aligned} \tag{8}$$

where

$$[\boldsymbol{D}_i]_k = -\frac{\partial[\boldsymbol{C}_i]_k}{\partial\alpha_{ki}} \tag{9}$$

Inasmuch as the inertia matrices for the rigid bodies are usually given in the body frame $\boldsymbol{b}$, it is convenient to assume that $[\boldsymbol{I}]$ is given in the body frame and to include the transformation to the $\hat{\boldsymbol{p}}$ frame in the equations

$$[\boldsymbol{I}^{\hat{p}}] = [\boldsymbol{T}][\boldsymbol{I}][\boldsymbol{T}]^T \tag{10}$$

where the notation $[\boldsymbol{I}^{\hat{p}}]$ is used whenever $[\boldsymbol{I}]$ is given in a frame different from the body frame.

B. Potential Energy

Because the dimensions of the probe and orbiter are very small compared with the size of the tethered system, they can be treated as particles in the potential energy computation. Therefore, the potential energies of the orbiter and the probe can be written as

$$V = -\mu\frac{m}{\sqrt{\{\boldsymbol{R}\}^T\{\boldsymbol{R}\}}} \tag{11}$$

where the corresponding position vectors are given in Eq. (3).

On the other hand, the tether elements may have very large dimensions, and the potential energy must be found by integrating along their lengths. However, this integration leads to singularities in certain orientations. To avoid this problem, we model the mass of the tether as being composed of two equal point masses located such that the moment of inertia is the same as for a rod [see Eq. (4)]. This model yields gravitational forces and moments within 1% of the rod model. Thus, the potential energy of each tether element can be written as

$$V_i = -\frac{\mu m_i}{2}\left(\frac{1}{\sqrt{\{\boldsymbol{R}_{i1}\}^T\{\boldsymbol{R}_{i1}\}}} + \frac{1}{\sqrt{\{\boldsymbol{R}_{i2}\}^T\{\boldsymbol{R}_{i2}\}}}\right) \tag{12}$$

For the spring associated with the ith rod, the potential energy is

$$V_{si} = \tfrac{1}{2}k_i x_i^2 \tag{13}$$

IV. Derivatives of Kinetic Energy

From Eqs. (2–10) the derivatives of kinetic energy with respect to $\dot{q}_j$ and q_j appearing in the equations of motion [Eq. (1)] for any body are

$$\begin{aligned}
&\frac{\mathrm{d}}{\mathrm{d}t}\left(\frac{\partial T}{\partial \dot{q}_j}\right) - \frac{\partial T}{\partial q_j} \\
&\quad = m\left\{\{\dot{\boldsymbol{v}}\}^T \frac{\partial\{\boldsymbol{v}\}}{\partial \dot{q}_j} + \{\boldsymbol{v}\}^T\left[\frac{\mathrm{d}}{\mathrm{d}t}\left(\frac{\partial\{\boldsymbol{v}\}}{\partial \dot{q}_j}\right) - \frac{\partial\{\boldsymbol{v}\}}{\partial q_j}\right]\right\} \\
&\quad + (\{\dot{\boldsymbol{\omega}}\}^T[\boldsymbol{T}] + \{\boldsymbol{\omega}\}^T[\dot{\boldsymbol{T}}])[\boldsymbol{I}][\boldsymbol{T}]^T \frac{\partial\{\boldsymbol{\omega}\}}{\partial \dot{q}_j} + \{\boldsymbol{\omega}\}^T[\boldsymbol{T}][\boldsymbol{I}] \\
&\quad \times\left\{[\dot{\boldsymbol{T}}]^T \frac{\partial\{\boldsymbol{\omega}\}}{\partial \dot{q}_j} + [\boldsymbol{T}]^T\left[\frac{\mathrm{d}}{\mathrm{d}t}\left(\frac{\partial\{\boldsymbol{\omega}\}}{\partial \dot{q}_j}\right) - \frac{\partial\{\boldsymbol{\omega}\}}{\partial q_j}\right] - \frac{\partial[\boldsymbol{T}]^T}{\partial q_j}\{\boldsymbol{\omega}\}\right\}
\end{aligned} \tag{14}$$

The time derivatives of the velocity vectors for the probe, the ith rod and the orbiter are

$$\begin{aligned}
\{\dot{\boldsymbol{v}}_p\} &= \{\ddot{\boldsymbol{R}}_p\} + [\tilde{\boldsymbol{\omega}}]\{\dot{\boldsymbol{R}}_p\} + [\dot{\tilde{\boldsymbol{\omega}}}]\{\boldsymbol{R}_p\} \\
\{\dot{\boldsymbol{v}}_i\} &= \{\ddot{\boldsymbol{R}}_p\} + [\tilde{\boldsymbol{\omega}}]\{\boldsymbol{v}_i\} + ([\dot{\tilde{\boldsymbol{\omega}}}] - [\tilde{\boldsymbol{\omega}}][\tilde{\boldsymbol{\omega}}])\{\boldsymbol{R}_{ic}\} \\
&\quad + [\ddot{\boldsymbol{T}}]_p\{\boldsymbol{r}_p\} + 2[\dot{\boldsymbol{T}}]_p\{\dot{\boldsymbol{r}}_p\} \\
&\quad + \sum_{k=1}^{i-1}([\ddot{\boldsymbol{T}}]_k\{\boldsymbol{l}_k\} + 2[\dot{\boldsymbol{T}}]_k\{\dot{\boldsymbol{x}}_k\} + [\boldsymbol{T}]_k\{\ddot{\boldsymbol{x}}_k\}) + \frac{1}{2}[\ddot{\boldsymbol{T}}]_i\{\boldsymbol{y}_i\}
\end{aligned} \tag{15}$$

$$\begin{aligned}
\{\dot{\boldsymbol{v}}_o\} &= \{\ddot{\boldsymbol{R}}_p\} + [\tilde{\boldsymbol{\omega}}]\{\boldsymbol{v}_o\} + ([\dot{\tilde{\boldsymbol{\omega}}}] - [\tilde{\boldsymbol{\omega}}][\tilde{\boldsymbol{\omega}}])\{\boldsymbol{R}_o\} \\
&\quad + [\ddot{\boldsymbol{T}}]_p\{\boldsymbol{r}_p\} + 2[\dot{\boldsymbol{T}}]_p\{\dot{\boldsymbol{r}}_p\} + \sum_{k=1}^{N}([\ddot{\boldsymbol{T}}]_k\{\boldsymbol{l}_k\} + 2[\dot{\boldsymbol{T}}]_k\{\dot{\boldsymbol{x}}_k\} \\
&\quad + [\boldsymbol{T}]_k\{\ddot{\boldsymbol{x}}_k\}) + [\ddot{\boldsymbol{T}}]_o\{\boldsymbol{r}_o\} + 2[\dot{\boldsymbol{T}}]_o\{\dot{\boldsymbol{r}}_o\}
\end{aligned}$$

where $[\dot{\boldsymbol{T}}]$ is given in Eq. (8) and

$$\begin{aligned}
[\ddot{\boldsymbol{T}}]_k &= -\ddot{\alpha}_1[\boldsymbol{D}_1]_k[\boldsymbol{C}_2]_k[\boldsymbol{C}_3]_k - \ddot{\alpha}_2[\boldsymbol{C}_1]_k[\boldsymbol{D}_2]_k[\boldsymbol{C}_3]_k \\
&\quad - \ddot{\alpha}_3[\boldsymbol{C}_1]_k[\boldsymbol{C}_2]_k[\boldsymbol{D}_3]_k - \dot{\alpha}_1^2[\boldsymbol{E}_1]_k[\boldsymbol{C}_2]_k[\boldsymbol{C}_3]_k \\
&\quad - \dot{\alpha}_2^2[\boldsymbol{C}_1]_k[\boldsymbol{E}_2]_k[\boldsymbol{C}_3]_k - \dot{\alpha}_3^2[\boldsymbol{C}_1]_k[\boldsymbol{C}_2]_k[\boldsymbol{E}_3]_k \\
&\quad + 2\dot{\alpha}_1\dot{\alpha}_2[\boldsymbol{D}_1]_k[\boldsymbol{D}_2]_k[\boldsymbol{C}_3]_k + 2\dot{\alpha}_1\dot{\alpha}_3[\boldsymbol{D}_1]_k[\boldsymbol{C}_2]_k[\boldsymbol{D}_3]_k \\
&\quad + 2\dot{\alpha}_2\dot{\alpha}_3[\boldsymbol{C}_1]_k[\boldsymbol{D}_2]_k[\boldsymbol{D}_3]_k
\end{aligned} \tag{16}$$

where

$$[\boldsymbol{E}_i]_k = \frac{\partial[\boldsymbol{D}_i]_k}{\partial\alpha_{ki}} \tag{17}$$

Next, partial derivatives of the velocities with respect to the q_j and $\dot{q}_j$ and their time derivatives are required. For R_p they are

$$\begin{aligned}
&\frac{\partial\{\boldsymbol{v}\}}{\partial \dot{R}_p} = \{1 \quad 0 \quad 0\}^T, \qquad \frac{\mathrm{d}}{\mathrm{d}t}\left(\frac{\partial\{\boldsymbol{v}\}}{\partial \dot{R}_p}\right) = \boldsymbol{0} \\
&\frac{\partial\{\boldsymbol{v}\}}{\partial R_p} = [\tilde{\boldsymbol{\omega}}]\{1 \quad 0 \quad 0\}^T
\end{aligned} \tag{18}$$

where $\{\boldsymbol{v}\}$ is $\{\boldsymbol{v}_p\}$, $\{\boldsymbol{v}_i\}$, or $\{\boldsymbol{v}_o\}$.

For ϕ

$$\begin{aligned}
&\frac{\partial\{\boldsymbol{v}_p\}}{\partial\phi} = \frac{\partial[\tilde{\boldsymbol{\omega}}]}{\partial\phi}\{\boldsymbol{R}_p\}, \qquad \frac{\partial\{\boldsymbol{v}_i\}}{\partial\phi} = \frac{\partial[\tilde{\boldsymbol{\omega}}]}{\partial\phi}\{\boldsymbol{R}_{ic}\} \\
&\frac{\partial\{\boldsymbol{v}_o\}}{\partial\phi} = \frac{\partial[\tilde{\boldsymbol{\omega}}]}{\partial\phi}\{\boldsymbol{R}_o\}
\end{aligned} \tag{19}$$

where

$$\frac{\partial[\tilde{\boldsymbol{\omega}}]}{\partial\dot{\phi}_1} = \begin{bmatrix} 0 & -\cos\phi_2 & 0 \\ \cos\phi_2 & 0 & \sin\phi_2 \\ 0 & -\sin\phi_2 & 0 \end{bmatrix}, \qquad \frac{\partial[\tilde{\boldsymbol{\omega}}]}{\partial\dot{\phi}_2} = \begin{bmatrix} 0 & 0 & 1 \\ 0 & 0 & 0 \\ -1 & 0 & 0 \end{bmatrix} \tag{20}$$

and

$$\begin{aligned}
\frac{\mathrm{d}}{\mathrm{d}t}\left(\frac{\partial\{\boldsymbol{v}_p\}}{\partial\dot{\phi}}\right) &= \frac{\mathrm{d}}{\mathrm{d}t}\left(\frac{\partial[\tilde{\boldsymbol{\omega}}]}{\partial\dot{\phi}}\right)\{\boldsymbol{R}_p\} + \frac{\partial[\tilde{\boldsymbol{\omega}}]}{\partial\dot{\phi}}\{\dot{\boldsymbol{R}}_p\} \\
\frac{\mathrm{d}}{\mathrm{d}t}\left(\frac{\partial\{\boldsymbol{v}_i\}}{\partial\dot{\phi}}\right) &= \frac{\mathrm{d}}{\mathrm{d}t}\left(\frac{\partial[\tilde{\boldsymbol{\omega}}]}{\partial\dot{\phi}}\right)\{\boldsymbol{R}_{ic}\} + \frac{\partial[\tilde{\boldsymbol{\omega}}]}{\partial\dot{\phi}}(\{\boldsymbol{v}_i\} - [\tilde{\boldsymbol{\omega}}]\{\boldsymbol{R}_{ic}\}) \\
\frac{\mathrm{d}}{\mathrm{d}t}\left(\frac{\partial\{\boldsymbol{v}_o\}}{\partial\dot{\phi}}\right) &= \frac{\mathrm{d}}{\mathrm{d}t}\left(\frac{\partial[\tilde{\boldsymbol{\omega}}]}{\partial\dot{\phi}}\right)\{\boldsymbol{R}_o\} + \frac{\partial[\tilde{\boldsymbol{\omega}}]}{\partial\dot{\phi}}(\{\boldsymbol{v}_o\} - [\tilde{\boldsymbol{\omega}}]\{\boldsymbol{R}_o\})
\end{aligned} \tag{21}$$

where

$$\begin{aligned}
&\frac{\mathrm{d}}{\mathrm{d}t}\left(\frac{\partial[\tilde{\boldsymbol{\omega}}]}{\partial\dot{\phi}_1}\right) = \begin{bmatrix} 0 & \dot{\phi}_2\sin\phi_2 & 0 \\ -\dot{\phi}_2\sin\phi_2 & 0 & \dot{\phi}_2\cos\phi_2 \\ 0 & -\dot{\phi}_2\cos\phi_2 & 0 \end{bmatrix} \\
&\frac{\mathrm{d}}{\mathrm{d}t}\left(\frac{\partial[\tilde{\boldsymbol{\omega}}]}{\partial\dot{\phi}_2}\right) = \boldsymbol{0}
\end{aligned} \tag{22}$$

$$\begin{aligned}
&\frac{\partial\{\boldsymbol{v}_p\}}{\partial\phi} = \frac{\partial[\tilde{\boldsymbol{\omega}}]}{\partial\phi}\{\boldsymbol{R}_p\}, \qquad \frac{\partial\{\boldsymbol{v}_i\}}{\partial\phi} = \frac{\partial[\tilde{\boldsymbol{\omega}}]}{\partial\phi}\{\boldsymbol{R}_{ic}\} \\
&\frac{\partial\{\boldsymbol{v}_o\}}{\partial\phi} = \frac{\partial[\tilde{\boldsymbol{\omega}}]}{\partial\phi}\{\boldsymbol{R}_o\}
\end{aligned} \tag{23}$$

and

$$\frac{\partial[\tilde{\boldsymbol{\omega}}]}{\partial\phi_1} = \boldsymbol{0}, \qquad \frac{\partial[\tilde{\boldsymbol{\omega}}]}{\partial\phi_2} = \begin{bmatrix} 0 & \dot{\phi}_1\sin\phi_2 & 0 \\ -\dot{\phi}_1\sin\phi_2 & 0 & \dot{\phi}_1\cos\phi_2 \\ 0 & -\dot{\phi}_1\cos\phi_2 & 0 \end{bmatrix} \tag{24}$$

For x_j, the displacement of the spring on the jth rod

$$\frac{\partial\{\boldsymbol{v}_p\}}{\partial\dot{x}_j} = \frac{\mathrm{d}}{\mathrm{d}t}\left(\frac{\partial\{\boldsymbol{v}_p\}}{\partial\dot{x}_j}\right) = \frac{\partial\{\boldsymbol{v}_p\}}{\partial x_j} = \boldsymbol{0} \tag{25}$$

$$\frac{\partial\{\boldsymbol{v}_i\}}{\partial\dot{x}_j} = \begin{cases} [\boldsymbol{T}]_j\{1 \quad 0 \quad 0\}^T & i > j \\ \boldsymbol{0} & i \le j \end{cases}$$

$$\frac{\mathrm{d}}{\mathrm{d}t}\left(\frac{\partial\{\boldsymbol{v}_i\}}{\partial\dot{x}_j}\right) = \begin{cases} [\dot{\boldsymbol{T}}]_j\{1 \quad 0 \quad 0\}^T & i > j \\ \boldsymbol{0} & i \le j \end{cases} \tag{26}$$

$$\frac{\partial\{\boldsymbol{v}_i\}}{\partial x_j} = \begin{cases} ([\dot{\boldsymbol{T}}]_j + [\tilde{\boldsymbol{\omega}}][\boldsymbol{T}]_j)\{1 \quad 0 \quad 0\}^T & i > j \\ \boldsymbol{0} & i \le j \end{cases}$$

$$\frac{\partial\{\boldsymbol{v}_o\}}{\partial\dot{x}_j} = [\boldsymbol{T}]_j\{1 \quad 0 \quad 0\}^T, \qquad \frac{\mathrm{d}}{\mathrm{d}t}\left(\frac{\partial\{\boldsymbol{v}_o\}}{\partial\dot{x}_j}\right) = [\dot{\boldsymbol{T}}]_j\{1 \quad 0 \quad 0\}^T \tag{27}$$

$$\frac{\partial\{\boldsymbol{v}_o\}}{\partial x_j} = ([\dot{\boldsymbol{T}}]_j + [\tilde{\boldsymbol{\omega}}][\boldsymbol{T}]_j)\{1 \quad 0 \quad 0\}^T$$

Next, derivatives are taken with respect to α_p. In this context α_p refers to α_{p1}, α_{p2}, and α_{p3} where the second subscript has been dropped because the three equations have the same form:

$$\frac{\partial\{\boldsymbol{v}_p\}}{\partial\dot{\alpha}_p} = \frac{\mathrm{d}}{\mathrm{d}t}\left(\frac{\partial\{\boldsymbol{v}_p\}}{\partial\dot{\alpha}_p}\right) = \frac{\partial\{\boldsymbol{v}_p\}}{\partial\alpha_p} = \boldsymbol{0} \tag{28}$$

$$\begin{aligned}
&\frac{\partial\{\boldsymbol{v}_i\}}{\partial\dot{\alpha}_p} = \frac{\partial\{\boldsymbol{v}_o\}}{\partial\dot{\alpha}_p} = \frac{\partial[\dot{\boldsymbol{T}}]_p}{\partial\dot{\alpha}_p}\{\boldsymbol{r}_p\} \\
&\frac{\mathrm{d}}{\mathrm{d}t}\left(\frac{\partial\{\boldsymbol{v}_i\}}{\partial\dot{\alpha}_p}\right) = \frac{\mathrm{d}}{\mathrm{d}t}\left(\frac{\partial\{\boldsymbol{v}_o\}}{\partial\dot{\alpha}_p}\right) = \frac{\mathrm{d}}{\mathrm{d}t}\left(\frac{\partial[\dot{\boldsymbol{T}}]_p}{\partial\dot{\alpha}_p}\right)\{\boldsymbol{r}_p\} + \frac{\partial[\dot{\boldsymbol{T}}]_p}{\partial\dot{\alpha}_p}\{\dot{\boldsymbol{r}}_p\} \\
&\frac{\partial\{\boldsymbol{v}_i\}}{\partial\alpha_p} = \frac{\partial\{\boldsymbol{v}_o\}}{\partial\alpha_p} = \left(\frac{\partial[\dot{\boldsymbol{T}}]_p}{\partial\alpha_p} + [\tilde{\boldsymbol{\omega}}]\frac{\partial[\boldsymbol{T}]_p}{\partial\alpha_p}\right)\{\boldsymbol{r}_p\} + \frac{\partial[\boldsymbol{T}]_p}{\partial\alpha_p}\{\dot{\boldsymbol{r}}_p\}
\end{aligned} \tag{29}$$

Similarly for the Euler angles of the orbiter α_{o1}, α_{o2}, and α_{o3},

$$\frac{\partial\{\boldsymbol{v}_p\}}{\partial\dot{\alpha}_o} = \frac{\partial\{\boldsymbol{v}_i\}}{\partial\dot{\alpha}_o} = \frac{\mathrm{d}}{\mathrm{d}t}\left(\frac{\partial\{\boldsymbol{v}_p\}}{\partial\dot{\alpha}_o}\right)$$

$$= \frac{\mathrm{d}}{\mathrm{d}t}\left(\frac{\partial\{\boldsymbol{v}_i\}}{\partial\dot{\alpha}_o}\right) = \frac{\partial\{\boldsymbol{v}_p\}}{\partial\alpha_o} = \frac{\partial\{\boldsymbol{v}_i\}}{\partial\alpha_o} = \boldsymbol{0} \tag{30}$$

$$\frac{\partial\{\boldsymbol{v}_o\}}{\partial\dot{\alpha}_o} = \frac{\partial[\dot{\boldsymbol{T}}]_o}{\partial\dot{\alpha}_o}\{\boldsymbol{r}_o\}$$

$$\frac{\mathrm{d}}{\mathrm{d}t}\left(\frac{\partial\{\boldsymbol{v}_o\}}{\partial\dot{\alpha}_o}\right) = \frac{\mathrm{d}}{\mathrm{d}t}\left(\frac{\partial[\dot{\boldsymbol{T}}]_o}{\partial\dot{\alpha}_o}\right)\{\boldsymbol{r}_o\} + \frac{\partial[\dot{\boldsymbol{T}}]_o}{\partial\dot{\alpha}_o}\{\dot{\boldsymbol{r}}_o\} \tag{31}$$

$$\frac{\partial\{\boldsymbol{v}_o\}}{\partial\alpha_o} = \left(\frac{\partial[\dot{\boldsymbol{T}}]_o}{\partial\alpha_o} + [\tilde{\boldsymbol{\omega}}]\frac{\partial[\boldsymbol{T}]_o}{\partial\alpha_o}\right)\{\boldsymbol{r}_o\} + \frac{\partial[\boldsymbol{T}]_o}{\partial\alpha_o}\{\dot{\boldsymbol{r}}_o\}$$

The partials of $[\boldsymbol{T}]_k$ and $[\dot{\boldsymbol{T}}]_k$ with respect to the α_k and their time derivatives are

$$\frac{\partial[\boldsymbol{T}]_k}{\partial\alpha_1} = \frac{\partial[\dot{\boldsymbol{T}}]_k}{\partial\dot{\alpha}_1} = -[\boldsymbol{D}_1]_k[\boldsymbol{C}_2]_k[\boldsymbol{C}_3]_k$$

$$\frac{\partial[\dot{\boldsymbol{T}}]_k}{\partial\alpha_1} = \frac{\mathrm{d}}{\mathrm{d}t}\left(\frac{\partial[\dot{\boldsymbol{T}}]_k}{\partial\dot{\alpha}_1}\right) = -\dot{\alpha}_1[\boldsymbol{E}_1]_k[\boldsymbol{C}_2]_k[\boldsymbol{C}_3]_k \tag{32}$$

$$+\dot{\alpha}_2[\boldsymbol{D}_1]_k[\boldsymbol{D}_2]_k[\boldsymbol{C}_3]_k + \dot{\alpha}_3[\boldsymbol{D}_1]_k[\boldsymbol{C}_2]_k[\boldsymbol{D}_3]_k$$

$$\frac{\partial[\boldsymbol{T}]_k}{\partial\alpha_2} = \frac{\partial[\dot{\boldsymbol{T}}]_k}{\partial\dot{\alpha}_2} = -[\boldsymbol{C}_1]_k[\boldsymbol{D}_2]_k[\boldsymbol{C}_3]_k$$

$$\frac{\partial[\dot{\boldsymbol{T}}]_k}{\partial\alpha_2} = \frac{\mathrm{d}}{\mathrm{d}t}\left(\frac{\partial[\dot{\boldsymbol{T}}]_k}{\partial\dot{\alpha}_2}\right) = \dot{\alpha}_1[\boldsymbol{D}_1]_k[\boldsymbol{D}_2]_k[\boldsymbol{C}_3]_k \tag{33}$$

$$-\dot{\alpha}_2[\boldsymbol{C}_1]_k[\boldsymbol{E}_2]_k[\boldsymbol{C}_3]_k + \dot{\alpha}_3[\boldsymbol{C}_1]_k[\boldsymbol{D}_2]_k[\boldsymbol{D}_3]_k$$

$$\frac{\partial[\boldsymbol{T}]_k}{\partial\alpha_3} = \frac{\partial[\dot{\boldsymbol{T}}]_k}{\partial\dot{\alpha}_3} = -[\boldsymbol{C}_1]_k[\boldsymbol{C}_2]_k[\boldsymbol{D}_3]_k$$

$$\frac{\partial[\dot{\boldsymbol{T}}]_k}{\partial\alpha_3} = \frac{\mathrm{d}}{\mathrm{d}t}\left(\frac{\partial[\dot{\boldsymbol{T}}]_k}{\partial\dot{\alpha}_3}\right) = \dot{\alpha}_1[\boldsymbol{D}_1]_k[\boldsymbol{C}_2]_k[\boldsymbol{D}_3]_k \tag{34}$$

$$+\dot{\alpha}_2[\boldsymbol{C}_1]_k[\boldsymbol{D}_2]_k[\boldsymbol{D}_3]_k - \dot{\alpha}_3[\boldsymbol{C}_1]_k[\boldsymbol{C}_2]_k[\boldsymbol{E}_3]_k$$

All other partials of $[\boldsymbol{T}]_k$ and $[\dot{\boldsymbol{T}}]_k$ are zero.

Finally, for the Euler angles of the jth tether element, α_{j1} and α_{j2},

$$\frac{\partial\{\boldsymbol{v}_p\}}{\partial\dot{\alpha}_j} = \frac{\mathrm{d}}{\mathrm{d}t}\left(\frac{\partial\{\boldsymbol{v}_p\}}{\partial\dot{\alpha}_j}\right) = \frac{\partial\{\boldsymbol{v}_p\}}{\partial\alpha_j} = \boldsymbol{0} \tag{35}$$

$$\frac{\partial\{\boldsymbol{v}_o\}}{\partial\dot{\alpha}_j} = \frac{\partial[\dot{\boldsymbol{T}}]_j}{\partial\dot{\alpha}_j}\{\boldsymbol{l}_j\}$$

$$\frac{\mathrm{d}}{\mathrm{d}t}\left(\frac{\partial\{\boldsymbol{v}_o\}}{\partial\dot{\alpha}_j}\right) = \frac{\mathrm{d}}{\mathrm{d}t}\left(\frac{\partial[\dot{\boldsymbol{T}}]_j}{\partial\dot{\alpha}_j}\right)\{\boldsymbol{l}_j\} + \frac{\partial[\dot{\boldsymbol{T}}]_j}{\partial\dot{\alpha}_j}\{\dot{\boldsymbol{x}}_j\} \tag{36}$$

$$\frac{\partial\{\boldsymbol{v}_o\}}{\partial\alpha_j} = \left(\frac{\partial[\dot{\boldsymbol{T}}]_j}{\partial\alpha_j} + [\tilde{\boldsymbol{\omega}}]\frac{\partial[\boldsymbol{T}]_j}{\partial\alpha_j}\right)\{\boldsymbol{l}_j\} + \frac{\partial[\boldsymbol{T}]_j}{\partial\alpha_j}\{\dot{\boldsymbol{x}}_j\}$$

$$\frac{\partial\{\boldsymbol{v}_i\}}{\partial\dot{\alpha}_j} = \begin{cases} \boldsymbol{0} & i < j \\ \dfrac{1}{2}\dfrac{\partial[\dot{\boldsymbol{T}}]_j}{\partial\dot{\alpha}_j}\{\boldsymbol{y}_j\} & i = j \\ \dfrac{\partial[\dot{\boldsymbol{T}}]_j}{\partial\dot{\alpha}_j}\{\boldsymbol{l}_j\} & i > j \end{cases}$$

$$\frac{\mathrm{d}}{\mathrm{d}t}\left(\frac{\partial\{\boldsymbol{v}_i\}}{\partial\dot{\alpha}_j}\right) = \begin{cases} \boldsymbol{0} & i < j \\ \dfrac{1}{2}\dfrac{\mathrm{d}}{\mathrm{d}t}\left(\dfrac{\partial[\dot{\boldsymbol{T}}]_j}{\partial\dot{\alpha}_j}\right)\{\boldsymbol{y}_j\} & i = j \\ \dfrac{\mathrm{d}}{\mathrm{d}t}\left(\dfrac{\partial[\dot{\boldsymbol{T}}]_j}{\partial\dot{\alpha}_j}\right)\{\boldsymbol{l}_j\} + \dfrac{\partial[\dot{\boldsymbol{T}}]_j}{\partial\dot{\alpha}_j}\{\dot{\boldsymbol{x}}_j\} & i > j \end{cases} \tag{37}$$

$$\frac{\partial\{\boldsymbol{v}_i\}}{\partial\alpha_j} = \begin{cases} \boldsymbol{0} & i < j \\ \dfrac{1}{2}\left(\dfrac{\partial[\dot{\boldsymbol{T}}]_j}{\partial\alpha_j} + [\tilde{\boldsymbol{\omega}}]\dfrac{\partial[\boldsymbol{T}]_j}{\partial\alpha_j}\right)\{\boldsymbol{y}_j\} & i = j \\ \left(\dfrac{\partial[\dot{\boldsymbol{T}}]_j}{\partial\alpha_j} + [\tilde{\boldsymbol{\omega}}]\dfrac{\partial[\boldsymbol{T}]_j}{\partial\alpha_j}\right)\{\boldsymbol{l}_j\} + \dfrac{\partial[\boldsymbol{T}]_j}{\partial\alpha_j}\{\dot{\boldsymbol{x}}_j\} & i > j \end{cases}$$

The partials of the inertial angular velocities with respect to the q_j and their time derivatives [required for Eqs. (14)] are

$$\frac{\partial\{\boldsymbol{\omega}\}}{\partial\dot{R}_p} = \frac{\partial\{\boldsymbol{\omega}\}}{\partial\dot{x}_j} = \boldsymbol{0}, \qquad \frac{\partial\{\boldsymbol{\omega}\}}{\partial\dot{\phi}_1} = \{-\sin\phi_2 \quad 0 \quad \cos\phi_2\}^T$$

$$\frac{\partial\{\boldsymbol{\omega}\}}{\partial\dot{\phi}_2} = \{0 \quad 1 \quad 0\}^T, \qquad \frac{\partial\{\boldsymbol{\omega}\}}{\partial\dot{\alpha}_1} = \{0 \quad 0 \quad 1\}^T \tag{38}$$

$$\frac{\partial\{\boldsymbol{\omega}\}}{\partial\dot{\alpha}_2} = \{-\sin\alpha_1 \quad \cos\alpha_1 \quad 0\}^T$$

$$\frac{\partial\{\boldsymbol{\omega}\}}{\partial\dot{\alpha}_3} = \{\cos\alpha_1\cos\alpha_2 \quad \sin\alpha_1\cos\alpha_2 \quad -\sin\alpha_2\}^T$$

$$\frac{\mathrm{d}}{\mathrm{d}t}\left(\frac{\partial\{\boldsymbol{\omega}\}}{\partial\dot{R}_p}\right) = \frac{\mathrm{d}}{\mathrm{d}t}\left(\frac{\partial\{\boldsymbol{\omega}\}}{\partial\dot{\phi}_2}\right) = \frac{\mathrm{d}}{\mathrm{d}t}\left(\frac{\partial\{\boldsymbol{\omega}\}}{\partial\dot{\alpha}_1}\right) = \frac{\mathrm{d}}{\mathrm{d}t}\left(\frac{\partial\{\boldsymbol{\omega}\}}{\partial\dot{x}_j}\right) = \boldsymbol{0}$$

$$\frac{\mathrm{d}}{\mathrm{d}t}\left(\frac{\partial\{\boldsymbol{\omega}\}}{\partial\dot{\phi}_1}\right) = \{-\dot{\phi}_2\cos\phi_2 \quad 0 \quad -\dot{\phi}_2\sin\phi_2\}^T, \qquad \frac{\mathrm{d}}{\mathrm{d}t}\left(\frac{\partial\{\boldsymbol{\omega}\}}{\partial\dot{\alpha}_2}\right) = \{-\dot{\alpha}_1\cos\alpha_1 \quad -\dot{\alpha}_1\sin\alpha_1 \quad 0\}^T \tag{39}$$

$$\frac{\mathrm{d}}{\mathrm{d}t}\left(\frac{\partial\{\boldsymbol{\omega}\}}{\partial\dot{\alpha}_3}\right) = \{-\dot{\alpha}_1\sin\alpha_1\cos\alpha_2 - \dot{\alpha}_2\cos\alpha_1\sin\alpha_2 \quad \dot{\alpha}_1\cos\alpha_1\cos\alpha_2 - \dot{\alpha}_2\sin\alpha_1\sin\alpha_2 \quad -\dot{\alpha}_2\cos\alpha_2\}^T$$

$$\frac{\partial\{\boldsymbol{\omega}\}}{\partial R_p} = \frac{\partial\{\boldsymbol{\omega}\}}{\partial\phi_1} = \frac{\partial\{\boldsymbol{\omega}\}}{\partial\alpha_3} = \frac{\partial\{\boldsymbol{\omega}\}}{\partial x_j} = \boldsymbol{0}, \qquad \frac{\partial\{\boldsymbol{\omega}\}}{\partial\phi_2} = \{-\dot{\phi}_1\cos\phi_2 \quad 0 \quad -\sin\phi_2\}^T$$

$$\frac{\partial\{\boldsymbol{\omega}\}}{\partial\alpha_1} = \{-\dot{\alpha}_2\cos\alpha_1 - \dot{\alpha}_3\sin\alpha_1\cos\alpha_2 \quad -\dot{\alpha}_2\sin\alpha_1 + \dot{\alpha}_3\cos\alpha_1\cos\alpha_2 \quad 0\}^T \tag{40}$$

$$\frac{\partial\{\boldsymbol{\omega}\}}{\partial\alpha_2} = \{-\dot{\alpha}_3\cos\alpha_1\sin\alpha_2 \quad -\dot{\alpha}_3\sin\alpha_1\sin\alpha_2 \quad -\dot{\alpha}_3\cos\alpha_2\}^T$$

V. Derivatives of Potential Energy

The derivatives of V with respect to q_j for the orbiter and the probe can be written as

$$\frac{\partial V}{\partial q_j} = \mu \frac{m}{R^3}\left(\{\boldsymbol{R}\}^T \frac{\partial \{\boldsymbol{R}\}}{\partial q_j}\right) \tag{41}$$

where

$$R = \sqrt{\{\boldsymbol{R}\}^T\{\boldsymbol{R}\}} \tag{42}$$

The respective position vectors are given in Eq. (3), and

$$\frac{\partial \{\boldsymbol{R}_p\}}{\partial q_j} = \begin{cases} \{1 \quad 0 \quad 0\}^T & q_j = R_p \\ \boldsymbol{0} & q_j \neq R_p \end{cases} \tag{43}$$

$$\frac{\partial \{\boldsymbol{R}_o\}}{\partial q_j} = \frac{\partial \{\boldsymbol{R}_p\}}{\partial q_j} + \frac{\partial [\boldsymbol{T}]_p}{\partial q_j}\{\boldsymbol{r}_p\} + \sum_{k=1}^{N}\left(\frac{\partial [\boldsymbol{T}]_k}{\partial q_j}\{\boldsymbol{l}_k\} + [\boldsymbol{T}]_k \frac{\partial \{\boldsymbol{l}_k\}}{\partial q_j}\right) + \frac{\partial [\boldsymbol{T}]_o}{\partial q_j}\{\boldsymbol{r}_o\} \tag{44}$$

Note that

$$\frac{\partial \{\boldsymbol{l}_k\}}{\partial q_j} = \begin{cases} \{1 \quad 0 \quad 0\}^T & q_j = x_k \\ \boldsymbol{0} & q_j \neq x_k \end{cases} \tag{45}$$

For the tether elements, Eq. (41) becomes

$$\frac{\partial V_i}{\partial q_j} = \frac{\mu m_i}{2}\left(\frac{1}{R_1^3}\{\boldsymbol{R}_{i1}\}^T \frac{\partial \{\boldsymbol{R}_{i1}\}}{\partial q_j} + \frac{1}{R_2^3}\{\boldsymbol{R}_{i2}\}^T \frac{\partial \{\boldsymbol{R}_{i2}\}}{\partial q_j}\right) \tag{46}$$

where the respective position vectors are given in Eq. (4) and

$$\frac{\partial \{\boldsymbol{R}_{i1}\}}{\partial q_j} = \frac{\partial \{\boldsymbol{R}_p\}}{\partial q_j} + \frac{\partial [\boldsymbol{T}]_p}{\partial q_j}\{\boldsymbol{r}_p\} + \sum_{k=1}^{i-1}\left(\frac{\partial [\boldsymbol{T}]_k}{\partial q_j}\{\boldsymbol{l}_k\} + [\boldsymbol{T}]_k \frac{\partial \{\boldsymbol{l}_k\}}{\partial q_j}\right) + \frac{3-\sqrt{3}}{6}\frac{\partial [\boldsymbol{T}]_i}{\partial q_j}\{\boldsymbol{y}_i\} \tag{47}$$

$$\frac{\partial \{\boldsymbol{R}_{i2}\}}{\partial q_j} = \frac{\partial \{\boldsymbol{R}_p\}}{\partial q_j} + \frac{\partial [\boldsymbol{T}]_p}{\partial q_j}\{\boldsymbol{r}_p\} + \sum_{k=1}^{i-1}\left(\frac{\partial [\boldsymbol{T}]_k}{\partial q_j}\{\boldsymbol{l}_k\} + [\boldsymbol{T}]_k \frac{\partial \{\boldsymbol{l}_k\}}{\partial q_j}\right) + \frac{3+\sqrt{3}}{6}\frac{\partial [\boldsymbol{T}]_i}{\partial q_j}\{\boldsymbol{y}_i\} \tag{48}$$

Note that all of the elements in Eqs. (44), (47), and (48) have already been computed in the preceding section.

For the potential energy of the spring associated with the ith rod, the derivatives are

$$\frac{\partial V_{si}}{\partial q_j} = \begin{cases} k_i x_i & q_j = x_i \\ 0 & q_j \neq x_i \end{cases} \tag{49}$$

VI. Generalized Forces

A. Drag Forces

To compute the aerodynamic forces acting on an element of the tether system, its wind velocity must be determined. Assuming the atmosphere rotates with the planet around the $\hat{\boldsymbol{e}}_3$ axis with angular velocity Ω, the atmospheric velocity at the location of the body of interest is

$$\{\boldsymbol{v}_{\text{atm}}\} = [\tilde{\boldsymbol{\Omega}}]\{\boldsymbol{R}\} \tag{50}$$

where $\{\boldsymbol{R}\}$ is the position vector to the element of interest and

$$[\tilde{\boldsymbol{\Omega}}] = \begin{bmatrix} 0 & -\Omega_3 & \Omega_2 \\ \Omega_3 & 0 & -\Omega_1 \\ -\Omega_2 & \Omega_1 & 0 \end{bmatrix}$$

is the rotation rate of the planet written in the probe frame. Therefore, the wind velocity of a particle moving with velocity $\{\boldsymbol{v}\}$ at a position determined by $\{\boldsymbol{R}\}$ is

$$\{\boldsymbol{v}_w\} = \{\boldsymbol{v}\} - \{\boldsymbol{v}_{\text{atm}}\} \tag{51}$$

1. Drag on a Sphere

To model the drag on the probe and orbiter, we will represent them as spheres with drag area S and coefficient of drag C_D. Substituting Eq. (51) for the wind velocity into

$$\{\boldsymbol{F}_{Ds}\} = -\tfrac{1}{2}\rho C_D S\sqrt{\{\boldsymbol{v}_w\}^T\{\boldsymbol{v}_w\}}\{\boldsymbol{v}_w\} \tag{52}$$

yields the drag force on the sphere. Given this drag force vector, the generalized force corresponding to the coordinate q_j is

$$Q_{jDs} = \{\boldsymbol{F}_{Ds}\}^T \frac{\partial \{\boldsymbol{R}\}}{\partial q_j} \tag{53}$$

where $\{\boldsymbol{R}\}$ is given in inertial coordinates.

The probe and orbiter can be treated as particles in this analysis because their dimensions are small. This means that Eq. (53) can be used directly with the corresponding positions and velocities given in Eqs. (3) and (7). The partial derivatives of $\{\boldsymbol{R}_p\}$ and $\{\boldsymbol{R}_o\}$ (written in the $\hat{\boldsymbol{e}}$ frame) appearing in the generalized forces are similar to the partial derivatives of $\{\boldsymbol{R}_p\}$ and $\{\boldsymbol{R}_o\}$ (written in the $\hat{\boldsymbol{p}}$ frame) in Eqs. (43) and (44). The only expression that is different for the generalized forces is

$$\frac{\partial \{\boldsymbol{R}\}}{\partial \phi} = [\boldsymbol{T}]_e^T \frac{\partial [\boldsymbol{T}]_e}{\partial \phi}\{\boldsymbol{R}\} \tag{54}$$

where partials with respect to ϕ are equivalent to partials with respect to α in Eqs. (33) and (34).

2. Drag on a Plate

To simply model the probe as a lifting body (possibly with fins), or to include the effects of solar panels on the orbiter, we will include the drag induced by a flat plate. For a plate with area A with its center of pressure located at $\{\boldsymbol{R}_{\text{cp}}\}$, the drag force on the plate is

$$\{\boldsymbol{F}_{Dp}\} = -2\rho A\left(\{\boldsymbol{v}_w\}^T\{\hat{\boldsymbol{n}}\}\right)\left|\{\boldsymbol{v}_w\}^T\{\hat{\boldsymbol{n}}\}\right|\{\hat{\boldsymbol{n}}\} \tag{55}$$

where

$$\{\hat{\boldsymbol{n}}\} = [\boldsymbol{T}]_p\{\hat{\boldsymbol{n}}_1 \quad \hat{\boldsymbol{n}}_2 \quad \hat{\boldsymbol{n}}_3\}^T \tag{56}$$

is the unit normal to the surface of the plate. Note that we have modeled the flow on the plate as being in full Newtonian flow, with perfect reflection of air particles with the plate (hence, the value of $C_D = 4$). The generalized force corresponding to the coordinate q_j is

$$Q_{jDp} = \{\boldsymbol{F}_{Dp}\}^T \frac{\partial \{\boldsymbol{R}_{\text{cp}}\}}{\partial q_j} \tag{57}$$

where the partials are evaluated as before.

3. Drag on the Tether

The analysis of the aerodynamic force on the tether is more complicated because each point of the tether is located at a different altitude, so that the density of the atmosphere varies along the tether length, and also because each point of the tether is moving at a different velocity with respect to the atmosphere. The differential force $\{\mathrm{d}\boldsymbol{F}_{Di}\}$ on the ith rod can be written as

$$\{\mathrm{d}\boldsymbol{F}_{Di}\} = -\tfrac{1}{2}\rho_{\xi i} C_D\sqrt{\{\boldsymbol{v}_{w\xi i}\}^T\{\boldsymbol{v}_{w\xi i}\}}\{\boldsymbol{v}_{w\xi i}\}\,\mathrm{d}S_\perp \tag{58}$$

where $\rho_{\xi i}$ is the atmospheric density at a distance of ξ along the ith rod, $\{\boldsymbol{v}_{w\xi i}\}$ is the velocity with respect to the atmosphere of the differential element at ξ on the ith rod, and $\mathrm{d}S_\perp$ is the cross-sectional differential area perpendicular to the wind direction.

We write the position vector to the differential element as

$$\{\boldsymbol{R}_{\xi i}\} = \{\boldsymbol{R}_p\} + [\boldsymbol{T}]_p\{\boldsymbol{r}_p\} + \sum_{k=1}^{i-1}[\boldsymbol{T}]_k\{\boldsymbol{l}_k\} + [\boldsymbol{T}]_i\{\xi \quad 0 \quad 0\}^T = \{\boldsymbol{B}_1\} + \{\boldsymbol{B}_2\}\xi \tag{59}$$

where $\{\boldsymbol{B}_1\}$ and $\{\boldsymbol{B}_2\}$ are used for convenience.

Then $\{\boldsymbol{v}_{w\xi i}\}$ can be written as

$$\{\boldsymbol{v}_{w\xi i}\} = \{\dot{\boldsymbol{R}}_p\} + [\dot{\boldsymbol{T}}]_p\{\boldsymbol{r}_p\} + [\boldsymbol{T}]_p\{\dot{\boldsymbol{r}}_p\} + \sum_{k=1}^{i-1}([\dot{\boldsymbol{T}}]_k\{\boldsymbol{l}_k\} + [\boldsymbol{T}]_k\{\dot{\boldsymbol{x}}_k\}) + [\boldsymbol{T}]_i\{\xi \quad 0 \quad 0\}^T + ([\tilde{\omega}] - [\tilde{\boldsymbol{\Omega}}])\{\boldsymbol{B}_1\} + \left([\dot{\boldsymbol{T}}]_i\{1 \quad 0 \quad 0\}^T + ([\tilde{\omega}] - [\tilde{\boldsymbol{\Omega}}])\{\boldsymbol{B}_2\}\right)\xi = \{\boldsymbol{D}_1\} + \{\boldsymbol{D}_2\}\xi \tag{60}$$

Assuming an exponential atmosphere, as already mentioned, and using the position vector of Eq. (59) we obtain

$$\rho_{\xi i} = \rho_r \exp\left[\frac{(h_r + R_{\rm pl})}{H}\right] \times \exp\left[-\frac{\sqrt{(\{\boldsymbol{B}_1\} + \{\boldsymbol{B}_2\}\xi)^T(\{\boldsymbol{B}_1\} + \{\boldsymbol{B}_2\}\xi)}}{H}\right] \tag{61}$$

where ρ_r is the density at the reference altitude h_r, H is the scale height of the atmosphere, and $R_{\rm pl}$ is the radius of the planet.

No closed-form expression in terms of elementary functions is possible for the integral $\int\{\mathrm{d}\boldsymbol{F}_{Di}\}$ when Eq. (61) is substituted into Eq. (58). However, very accurate, closed-form, approximate solutions can be found by assuming

$$\exp\left[-\frac{\sqrt{(\{\boldsymbol{B}_1\} + \{\boldsymbol{B}_2\}\xi)^T(\{\boldsymbol{B}_1\} + \{\boldsymbol{B}_2\}\xi)}}{H}\right] \approx \exp\left[-\frac{\|\{\boldsymbol{B}_1\}\|}{H}\right]\exp\left[-\frac{\xi\cos\alpha_{i1}\cos\alpha_{i2}}{H}\right] \tag{62}$$

which is equivalent to arithmetically adding the $\hat{\boldsymbol{p}}_1$ projection of $\{\boldsymbol{B}_2\}$ to $\{\boldsymbol{B}_1\}$. Thus, Eq. (61) becomes

$$\rho_{\xi i} = \rho_r \exp\left[\frac{(h_r + R_{\rm pl} - \|\{\boldsymbol{B}_1\}\|)}{H}\right]\exp\left[-\frac{\xi\cos\alpha_{i1}\cos\alpha_{i2}}{H}\right] = K\exp\left[-\frac{\xi\cos\alpha_{i1}\cos\alpha_{i2}}{H}\right] \tag{63}$$

where K is a convenient coefficient.

Finally, the differential area can be expressed as

$$\mathrm{d}S_\perp = \frac{\|\{\boldsymbol{v}_{w\xi i}\} \times \hat{\boldsymbol{b}}_1\|}{\|\{\boldsymbol{v}_{w\xi i}\}\|} d_i\,\mathrm{d}\xi \tag{64}$$

where d_i is the diameter of the tether element and $\hat{\boldsymbol{b}}_1$ is aligned with the tether element.

Again, however, no closed-form solution exists for $\int\{\mathrm{d}\boldsymbol{F}_{Di}\}$ when Eq. (64) is substituted into Eq. (58). To rectify this problem we assume the angle between the rod and the velocity vector relative to the wind is constant along the length of the rod. Then $\mathrm{d}S_\perp$ can be written as

$$\mathrm{d}S_\perp = \frac{\|\{\boldsymbol{v}_{w\mathrm{ref}}\} \times \hat{\boldsymbol{b}}_1\|}{\|\{\boldsymbol{v}_{w\mathrm{ref}}\}\|} d_i\,\mathrm{d}\xi \tag{65}$$

where the reference velocity $\{\boldsymbol{v}_{w\mathrm{ref}}\}$ is chosen to be the velocity at the center of mass of the rod.

One last assumption must be employed before Eq. (58) can be integrated. The velocity term under the radical is assumed to be constant, and so we set

$$\sqrt{\{\boldsymbol{v}_{w\xi i}\}^T\{\boldsymbol{v}_{w\xi i}\}} \approx \sqrt{\{\boldsymbol{v}_{w\mathrm{ref}}\}^T\{\boldsymbol{v}_{w\mathrm{ref}}\}} \tag{66}$$

where, again, the reference velocity is usually chosen to be at the center of mass of each rod.

The validity of these assumptions increases as the rod lengths are shortened. As the lengths of the rods become arbitrarily small, the expressions are exact.

Substituting Eqs. (63), (65), and (66) into Eq. (58) yields the approximate differential drag force

$$\{\mathrm{d}\boldsymbol{F}_{Di}\} = -\frac{1}{2}C_D K d_i \|\{\boldsymbol{v}_{w\mathrm{ref}}\} \times \hat{\boldsymbol{b}}_1\|(\{\boldsymbol{D}_1\} + \{\boldsymbol{D}_2\}\xi) \times \exp\left[-\frac{\xi\cos\alpha_{i1}\cos\alpha_{i2}}{H}\right]\mathrm{d}\xi \tag{67}$$

To obtain the generalized forces the following expression is employed:

$$Q_{ji} = \int_0^{y_i}\{\mathrm{d}\boldsymbol{F}_{Di}\}^T\frac{\partial\{\boldsymbol{R}_{\xi i}\}}{\partial q_j} \tag{68}$$

where the partial derivatives of $\{\boldsymbol{R}_{\xi i}\}$ are

$$\frac{\partial\{\boldsymbol{R}_{\xi i}\}}{\partial\phi} = [\boldsymbol{T}]_e^T\frac{\partial[\boldsymbol{T}]_e}{\partial\phi}\{\boldsymbol{R}_{\xi i}\}$$

$$\frac{\partial\{\boldsymbol{R}_{\xi i}\}}{\partial R_p} = \{1 \quad 0 \quad 0\}^T, \qquad \frac{\partial\{\boldsymbol{R}_{\xi i}\}}{\partial\alpha_p} = \frac{\partial[\boldsymbol{T}]_p}{\partial\alpha_p}\{\boldsymbol{r}_p\}$$

$$\frac{\partial\{\boldsymbol{R}_{\xi i}\}}{\partial\alpha_j} = \begin{cases}\dfrac{\partial[\boldsymbol{T}]_j}{\partial\alpha_j}\{\boldsymbol{l}_j\} & i > j\\ \dfrac{\partial[\boldsymbol{T}]_j}{\partial\alpha_j}\{1 \quad 0 \quad 0\}^T\xi & i = j\\ \{0 \quad 0 \quad 0\}^T & i < j\end{cases} \tag{69}$$

$$\frac{\partial\{\boldsymbol{R}_{\xi i}\}}{\partial\alpha_o} = \{0 \quad 0 \quad 0\}^T$$

$$\frac{\partial\{\boldsymbol{R}_{\xi i}\}}{\partial x_j} = \begin{cases}[\boldsymbol{T}]_j\{1 \quad 0 \quad 0\}^T & i > j\\ \{0 \quad 0 \quad 0\}^T & i \le j\end{cases}$$

Substituting Eqs. (67) and (69) into Eq. (68) and integrating yields the following expressions for the generalized forces:

$$Q_{\phi i} = -\frac{1}{2}C_D K d_i\|\{\boldsymbol{v}_{w\mathrm{ref}}\} \times \hat{\boldsymbol{b}}_1\|\left[\{\boldsymbol{D}_1\}^T[\boldsymbol{T}]_e^T\frac{\partial[\boldsymbol{T}]_e}{\partial\phi} \times (\{\boldsymbol{B}_1\}I_0 + \{\boldsymbol{B}_2\}I_1) + \{\boldsymbol{D}_2\}^T[\boldsymbol{T}]_e^T\frac{\partial[\boldsymbol{T}]_e}{\partial\phi}(\{\boldsymbol{B}_1\}I_1 + \{\boldsymbol{B}_2\}I_2)\right]$$

$$Q_{R_p i} = -\tfrac{1}{2}C_D K d_i\|\{\boldsymbol{v}_{w\mathrm{ref}}\} \times \hat{\boldsymbol{b}}_1\|\left[\{\boldsymbol{D}_1\}^T I_0 + \{\boldsymbol{D}_2\}^T I_1\right]\{1 \quad 0 \quad 0\}^T$$

$$Q_{\alpha_p i} = -\frac{1}{2}C_D K d_i\|\{\boldsymbol{v}_{w\mathrm{ref}}\} \times \hat{\boldsymbol{b}}_1\|\left[\{\boldsymbol{D}_1\}^T I_0 + \{\boldsymbol{D}_2\}^T I_1\right]\frac{\partial[\boldsymbol{T}]_p}{\partial\alpha_p}\{\boldsymbol{r}_p\}$$

$$Q_{\alpha_j i} = \begin{cases}-\dfrac{1}{2}C_D K d_i\|\{\boldsymbol{v}_{w\mathrm{ref}}\} \times \hat{\boldsymbol{b}}_1\| \times\left[\{\boldsymbol{D}_1\}^T I_0 + \{\boldsymbol{D}_2\}^T I_1\right]\dfrac{\partial[\boldsymbol{T}]_j}{\partial\alpha_j}\{\boldsymbol{l}_j\} & i > j\\ -\dfrac{1}{2}C_D K d_i\|\{\boldsymbol{v}_{w\mathrm{ref}}\} \times \hat{\boldsymbol{b}}_1\| \times\left[\{\boldsymbol{D}_1\}^T I_1 + \{\boldsymbol{D}_2\}^T I_2\right]\dfrac{\partial[\boldsymbol{T}]_j}{\partial\alpha_j}\{1 \quad 0 \quad 0\}^T & i = j\\ 0 & i < j\end{cases}$$

$$Q_{\alpha_o i} = 0$$

$$Q_{x_j i} = \begin{cases}-\dfrac{1}{2}C_D K d_i\|\{\boldsymbol{v}_{w\mathrm{ref}}\} \times \hat{\boldsymbol{b}}_1\| \times\left[\{\boldsymbol{D}_1\}^T I_0 + \{\boldsymbol{D}_2\}^T I_1\right][\boldsymbol{T}]_j\{1 \quad 0 \quad 0\}^T & i > j\\ -c_i\dot{x}_i & i = j\\ 0 & i < j\end{cases} \tag{70}$$

where

$$I_n = \int_0^{y_i} \xi^n \exp\left[-\frac{\xi \cos\alpha_{i1} \cos\alpha_{i2}}{H}\right] d\xi \qquad (71)$$

The I_n are known integrals, which are discussed in Refs. 4 and 5.

Note that, although the atmospheric density profile presented here is a uniform exponential, more advanced models could be readily incorporated. An improvement would be to use a variable scale height model, where the scale height used in the integral becomes a function of the altitude of the tether segment. The drag then is computed using the appropriate scale height and density for each tether segment. In this case, as the number of tether elements increases, so does the accuracy of the drag computation. It is, of course, possible to use an exact atmospheric model,[20] but the drag would then need to be numerically integrated.

VII. Numerical Results

This new, more realistic model is used to provide further verification of the feasibility of aerobraking with tethers. The simulation shown here involves a three-rod tether model including springs, dampers, and rigid-body end masses. It is based on an optimal tether mass aerocapture[9] designed with a planar, rigid-rod model. The characteristics of this system are shown in Table 1.

The initial orbit is based on a Hohmann transfer from Earth to Mars that lies in the ecliptic plane. The resulting arrival orbit with respect to Mars is defined by the parameters listed in Table 2. The initial orientation and spin rate of the system outside the atmosphere must be chosen carefully so that aerocapture is achieved. For this case, $\alpha_0 = 280.7$ deg and $\dot{\alpha}_0 = -0.01703$ rad/s when the center of mass of the system is located at $r_{\text{c.m.}}$ in Table 2.

The results of the simulation are given in Figs. 3–9. The orientations of the three rods within the orbital plane with respect to the local vertical are plotted in Fig. 3. The rods are aligned prior to impact with the atmosphere. Near periapsis (around 250 s), separation in the curves indicates significant bending, but this effect is damped out as the system exits the atmosphere. These results are very similar to those of the rigid-planar model[9] and of the flexible-planar model.[11] This confirms that the rigid model is useful as a design tool.

The out-of-plane displacements of the tether segments are shown in Fig. 4. Out-of-plane components of wind velocity due to the inclination of the orbit induce these oscillations. Note, however, that in this case, the effect is small and does not significantly alter the maneuver. This verifies that the standard assumption to neglect out-of-plane effects is reasonable.

The magnitude of the forces exerted on the tether at the orbiter (Fig. 5) are also consistent with the planar, rigid-rod model. Note that the force in the tether slightly exceeds the breaking strength (shown as the dash-dot line). The diameter of the flexible tether needs to be modified slightly from the rigid design to handle these loads, along with a suitable factor of safety.

Figure 6 shows the orientation of the probe during the maneuver. It rotates with the tether until it impacts the atmosphere where some additional rotation is imparted by the atmospheric forces. The oscillations of the probe are small and of no major concern. This verifies that the probe is well behaved as it enters the atmosphere.

Near periapsis, the orbiter hovers near a radius of 3480 km (an altitude of 82 km) while the probe continues farther into the atmosphere (Fig. 7). The greatest bending of the system occurs during this phase of the maneuver, where the drag on the tether dominates. Note that without the tether, a point mass performing this same maneuver would have to pass through the atmosphere at the altitude of the

Table 1 System parameters

Tether mass	64.47 kg
Probe mass	1000 kg
Orbiter mass	1000 kg
Tether length	21.05 km
Tether diameter	1.472 mm
Probe area	100 m^2

Table 2 Orbital parameters

V_∞	2.649 km/s
r_p	3472.8 km
i	24 deg
ω	0 deg
Ω	0 deg
$r_{\text{c.m.}}$	3654.0 km

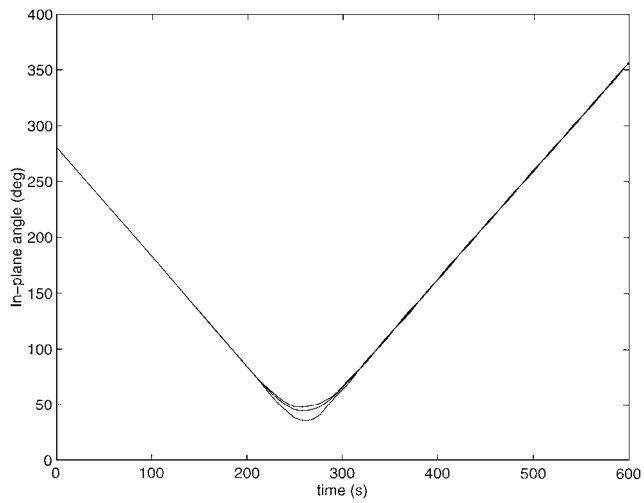

Fig. 3 In-plane orientation.

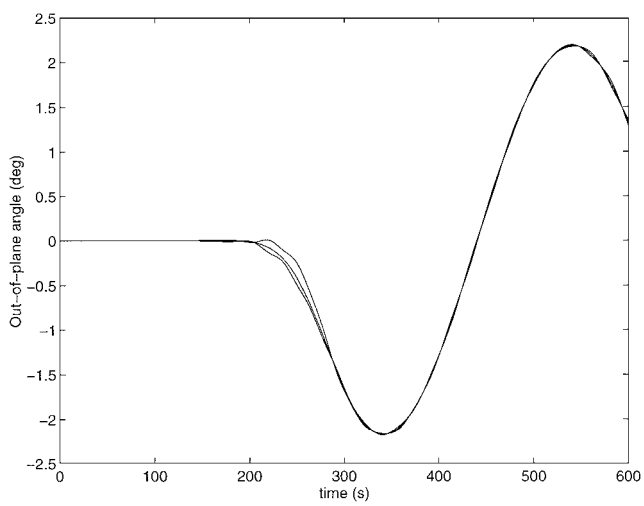

Fig. 4 Out-of-plane orientation.

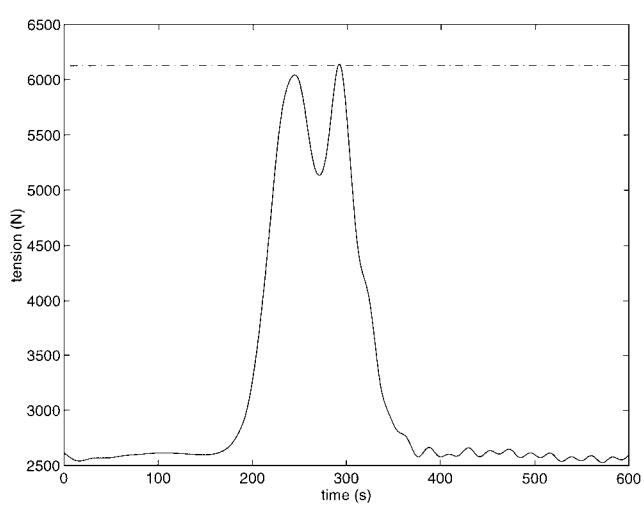

Fig. 5 Tether forces at orbiter.

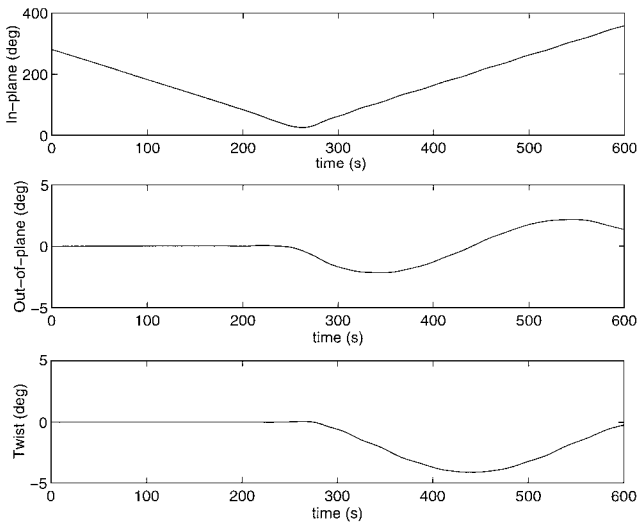

Fig. 6 Rigid-body probe orientation.

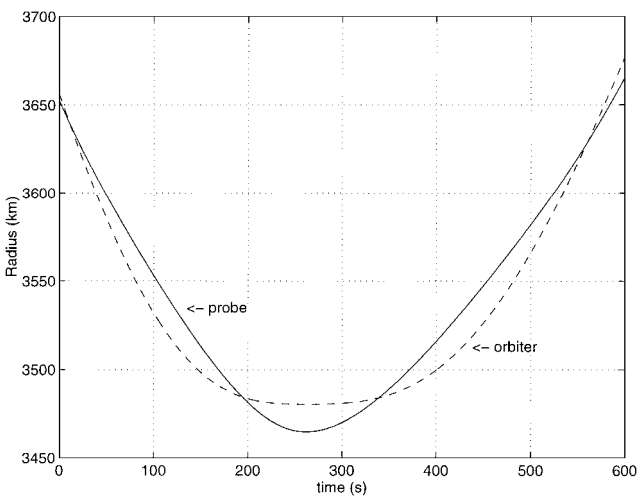

Fig. 7 Radius of probe and orbiter.

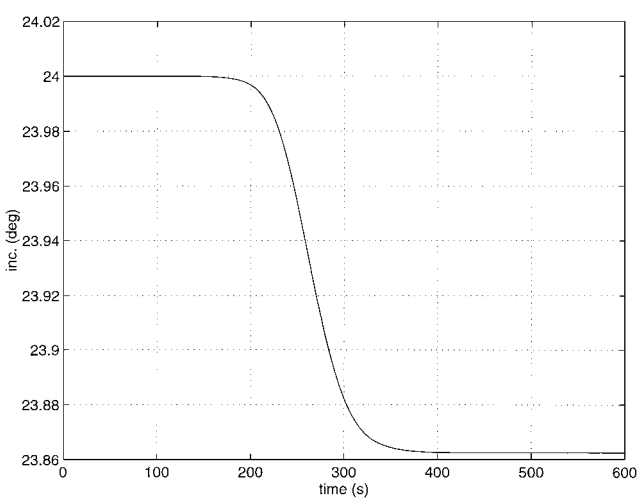

Fig. 8 Orbital inclination.

probe (62 km), requiring significantly more thermal shielding. The design used here required a clearance of 1.8 scale heights between the minimum altitudes of the probe and orbiter. Using a longer tether would result in less heating at the orbiter and even greater heat shield savings. The orbiter would be even higher above the atmosphere, and the additional tether area would aid in braking.

This model permits the observation of inclination changes shown in Fig. 8. Crosswinds encountered in this nonequatorial orbit produce a slight decrease in the inclination. This suggests that it may be possible to use repeated passes with the tether system to significantly change the inclination of the orbit.

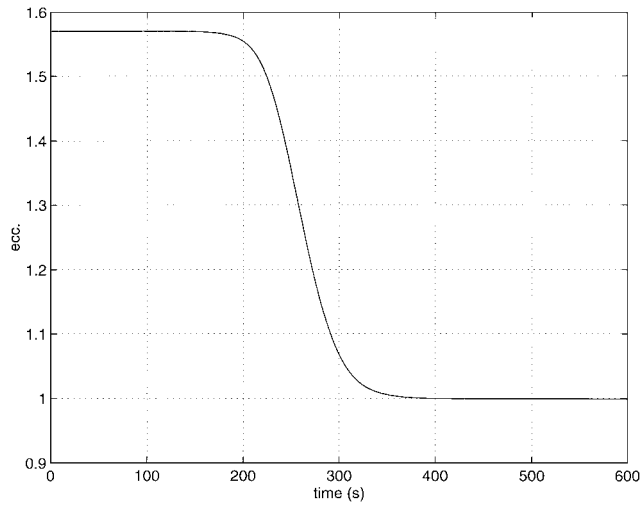

Fig. 9 Orbital eccentricity.

After the maneuver, the system is captured about Mars ($e_{\text{final}} = 0.9992$) even when flexibility and out-of-plane effects are included (Fig. 9). Thus, the feasibility of hyperbolic aerocapture with tethers is further validated by this new model.

The results presented here were derived using only three tether elements in the simulation. However, additional simulations were performed with as many as 10 elements, with minimal change to the results. This small number of elements serves to clearly show the behavior of the flexible system, without the computational cost of a large system.

VIII. Conclusions

The new model presented here provides a high-fidelity simulation tool for aerobraking tethers. Its greatest strength lies in the ability to accurately model the aerodynamic and gravitational forces and moments with only a limited number of elements (even as few as 1) as opposed to the large number of beads required to achieve the same results. This reduces the computational cost by reducing the order of the model. In addition, the formulation is ideal for numerical simulation, presenting the equations in a compact and easily programmable form. This new model may provide a valuable tool for researchers studying tether systems in the atmosphere.

The results presented clearly show that the rigid-rod model is a useful design tool in the development of aerocapture-type maneuvers. The optimal design from the rigid model requires only limited manipulation to handle the effects of flexibility and elasticity. The results indicate that, for the case presented, probe behavior (modeled here for the first time) is benign and does not interfere with the aerocapture maneuver. Overall, the aerocapture maneuver remains feasible even when considering the additional dynamics included in this high-fidelity simulation.

References

[1] Carroll, J. A., "Tether Applications in Space Transportation," *Acta Astronautica*, Vol. 13, No. 4, 1986, pp. 165–174 .

[2] Sirlin, S. W., Laskin, R. A., Otake, H., and Longuski, J. M., "Proposal to JPL Director's Discretionary Fund FY '84: Tethers for Aerocapture and Trajectory Maneuvers," Jet Propulsion Lab., California Inst. of Technology, Pasadena, CA, Aug. 1984.

[3] Purvis, C., and Penzo, P., "Multipass Aerobraking of Planetary Probe," *Tethers in Space Handbook*, Office of Space Flight Advanced Programs, NASA, 1986.

[4] Puig-Suari, J., and Longuski, J. M., "Modeling and Analysis of Tethers in an Atmosphere," *Acta Astronautica*, Vol. 25, No. 11, 1991, pp. 679–686.

[5] Longuski, J. M., and Puig-Suari, J., "Hyperbolic Aerocapture and Elliptic Orbit Transfer with Tethers," 42nd International Astronautical Federation Congress, IAF Paper 91-339, Montreal, PQ, Canada, Oct. 1991.

[6] Lorenzini, E., Grossi, M. D., and Cosmo, M., "Low Altitude Tethered Mars Probe," *Acta Astronautica*, Vol. 21, No. 1, 1990, pp. 1–12.

[7]Puig-Suari, J., and Longuski, J. M., "Analysis of Aerocapture with Tethers," American Astronautical Society/AIAA Astrodynamics Conf., AAS Paper 91-549, Durango, CO, Aug. 1991.

[8]Puig-Suari, J., Longuski, J. M., and Mechalas, J., "Aerobraking Tethers for the Exploration of the Solar System," *Acta Astronautica*, Vol. 35, No. 2/3, 1995, pp. 205–214.

[9]Longuski, J. M., Puig-Suari, J., Tsiotras, P., and Tragesser, S., "Optimal Mass for Aerobraking Tethers," 44th International Astronautical Federation Congress, IAF Paper 93-A.2.13, Graz, Austria, Oct. 1993.

[10]Puig-Suari, J., and Longuski, J. M., "Aerocapture with a Flexible Tether," AIAA Paper 92-4662, Aug. 1992.

[11]Puig-Suari, J., "Optimal Mass Flexible Tethers for Aerobraking Maneuvers," Fourth International Conf. on Tethers in Space, Paper ThDYNp-8, Washington, DC, April 1995.

[12]Penzo, P. A., and Ammann, P. W. (eds.), *Tethers in Space Handbook*, 2nd ed., Office of Space Flight Advanced Programs, NASA, 1989.

[13]He, X., and Powell, J. D., "Tether Damping in Space," International Conf. on Tethers in Space, Venice, Italy, AIAA/NASA/ASI/ESA, Oct. 1987.

[14]Lemke, L. G., Powell, J. D., and He, X., "Attitude Control of Tethered Spacecraft," *Journal of the Astronautical Sciences*, Vol. 35, No. 1, 1987, pp. 41–55.

[15]Kline-Schoder, R., and Powell, J. D., "Experiments with the KITE Attitude Control Simulator," AIAA Paper 89-1576, May 1989.

[16]Banerjee, A., and Kline-Schoder, R., "Attitude Control of an Orbiting Tethered Gyrostat," AIAA Paper 92-4664, Aug. 1992.

[17]Banerjee, A. K., and Kane, T. R., "Pointing Control, with Tethers as Actuators, of a Space Station Supported Platform," *Journal of Guidance, Control, and Dynamics*, Vol. 16, No. 2, 1993, pp. 396–399.

[18]Moccia, A., Vetrella, S., and Grassi, M., "Attitude Dynamics and Control of a Vertical Interferometric Radar Tether Altimeter," *Journal of Guidance, Control, and Dynamics*, Vol. 16, No. 2, 1993, pp. 264–269.

[19]Arnold, D. A., "The Behavior of Long Tethers in Space," *Journal of the Astronautical Sciences*, Vol. 35, No. 1, 1987, pp. 3–18.

[20]Bergamaschi, S., and Bonon, F., "Equilibrium Configurations in a Tethered Atmospheric Mission," American Astronautical Society/AIAA Astrodynamics Conf., AAS Paper 91-543, Durango, CO, Aug. 1991.

[21]Keshmiri, M., and Misra, A. K., "Effects of Aerodynamic Lift on the Stability of Tethered Subsatellite Systems," American Astronautical Society/AIAA Spaceflight Mechanics Meeting, AAS Paper 93-184, Pasadena, CA, Feb. 1993.

[22]Gullahorn, G., "Atmospheric Density Variations Via Tethered Satellite Drag," AIAA Paper 89-1566, May 1989.

[23]Krischke, M., Lorenzini, E., and Sabath, D., "A Hypersonic Parachute for Low-Temperature Reentry," 43rd International Astronautical Federation Congress, IAF Paper 92-0822, Washington, DC, Aug.–Sept. 1992.

[24]Pasca, M., and Lorenzini, E. C., "Collection of Martian Atmospheric Dust with a Low Altitude Tethered Probe," American Astronautical Society/AIAA Spaceflight Mechanics Meeting, AAS Paper 91-178, Houston, TX, Feb. 1991.

[25]Bae, G., Sim, E., and Barlow, J. B., "The Atmospheric Flight Equations of a Tethered Hypersonic Waverider," American Astronautical Society/AIAA Spaceflight Mechanics Meeting, AAS Paper 93-185, Pasadena, CA, Feb. 1993.

[26]Warnock, T. W., and Cochran, J. E., "Predicting the Orbital Lifetime of Tethered Satellite Systems," 43rd International Astronautical Federation Congress, IAF Paper 92-0002, Washington, DC, Aug.–Sept. 1992.

[27]Von Flotow, A. H., "Some Approximations for the Dynamics of Spacecraft Tethers," *Journal of Guidance, Control, and Dynamics*, Vol. 11, No. 4, 1988, pp. 357–364.

[28]Von Flotow, A. H., and Wereley, N. M., "Coupling of Tether Modes with Sub-Satellite Attitude Motion," American Astronautical Society/AIAA Astrodynamics Conf., AAS Paper 87-433, Kalispell, MT, Aug. 1987.

[29]Etter, J. R., and Hedding, L. R., "An Experimental Investigation of the Longitudinal Dynamics of Long Kevlar Tethers," AIAA Paper 92-4663, Aug. 1992.

[30]Harrison, J. K., Rupp, C. C., Carroll, J. A., Alexander, C. M., and Pulliam, E. R., "Small Expendable-Deployer System (SEDS) Development Status," AIAA Paper 89-1550, May 1989.

[31]Crouch, D. S., Van Pelt, J. M., and Flanders, H. A., "A Titan II-Based Tethered Satellite System," 42nd International Astronautical Federation Congress, IAF Paper 91-004, Montreal, Canada, PQ, Oct. 1991.

[32]Tyc, G., Hans, R. P. S., Vigneron, F. R., Modi, V. J., Misra, A. K., and Berry, T. G., "Tether Dynamics Investigations for the Canadian Oedipus Sounding Rocket Program," AIAA Paper 92-4672, Aug. 1992.

[33]No, T. S., and Cochran, J. E., "Dynamics and Control of a Tethered Flight Vehicle," American Astronautical Society/AIAA Astrodynamics Conf., AAS Paper 91-544, Durango, CO, Aug. 1991.

[34]Breakwell, J. V., and Gearhart, J. M., "Pumping a Tethered Configuration to Boost Its Orbit Around an Oblate Planet," *Journal of the Astronautical Sciences*, Vol. 35, No. 1, 1987, pp. 19–39.

[35]Landis, G. A., "Reactionless Orbital Propulsion Using Tether Deployment," 41st International Astronautical Federation Congress, IAF Paper 90-254, Dresden, Germany, Oct. 1990.

[36]Anderson, K., and Hagedorn, P., "On the Control of Orbital Drift of Geostationary Tethered Satellites," 43rd International Astronautical Federation Congress, IAF Paper 92-0003, Washington, DC, Aug.–Sept. 1992.

[37]Lang, D., "GTOSS (Generalized Tether Object Simulation System)," *Tether Dynamics Simulation*, NASA CP 2458, 1987.

[38]Puig-Suari, J., Longuski, J. M., and Tragesser, S., "A Three Dimensional Hinged-Rod Model for Flexible-Elastic Aerobraking Tethers," American Astronautical Society/AIAA Astrodynamics Conf., AAS Paper 93-730, Victoria, BC, Canada, Aug. 1993.

[39]Biswell, B., and Puig-Suari, J., "Lifting Body Effects on the Equilibrium Orientation of Tethers in the Atmosphere," AIAA Paper 96-3598, July 1996.